Electronic Supplementary Material (ESI) for Lab on a Chip.

Supplementary Information

Supplementary Table 1 | Detection limit and density testing

	CD34+ cells per µL	
	Magnetophoretic Cytometry	Flow Cytometry Control
Sample 1	3.08	5.82
Sample 2	4.01	4.91
Sample 3	9.44	10.54
Sample 4	5.35	5.21
Sample 5	1.92	1.79
Sample 6	2.07	4.58
Sample 7	2.49	5.37
Sample 8	2.27	3.16
Sample 9	3.67	8.17
Sample 10	5.02	5.99
Sample 11	23.32	22.68

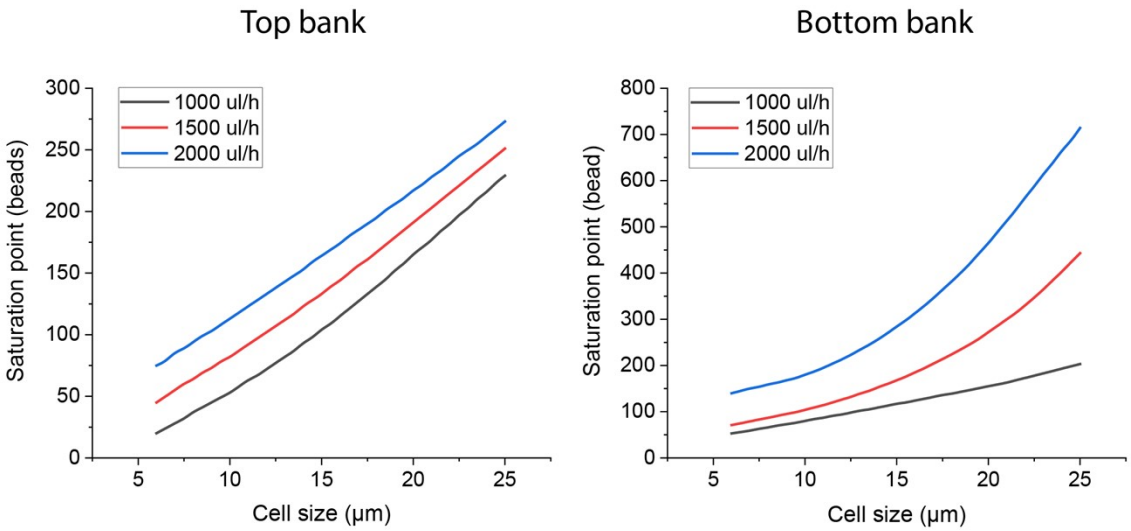

Supplementary Figure 1 | Dynamic range limits for the top and bottom sensor banks versus the cell size under different flow rates.

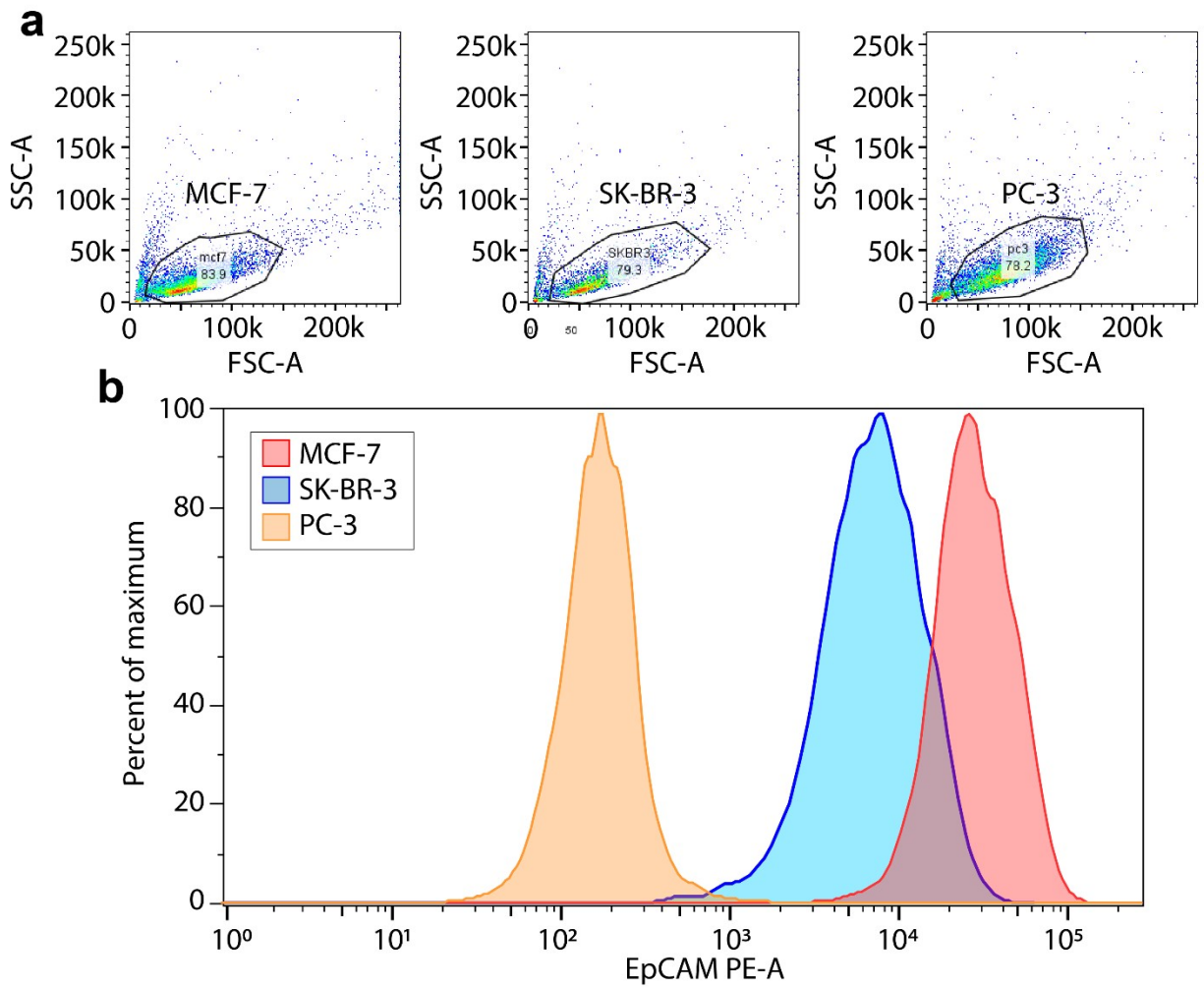

Supplementary Figure 2 | Flow cytometry analysis of PC-3, SK-BR-3, and MCF-7 cancer cell lines. (**a**) The live cells were gated using forward scatter versus side scatter plots to eliminate debris from the samples of MCF-7, SK-BR-3, and PC-3 cells. (**b**) MCF-7 cells showed the highest EpCAM expression, while PC-3 showed the least among the three cell lines.

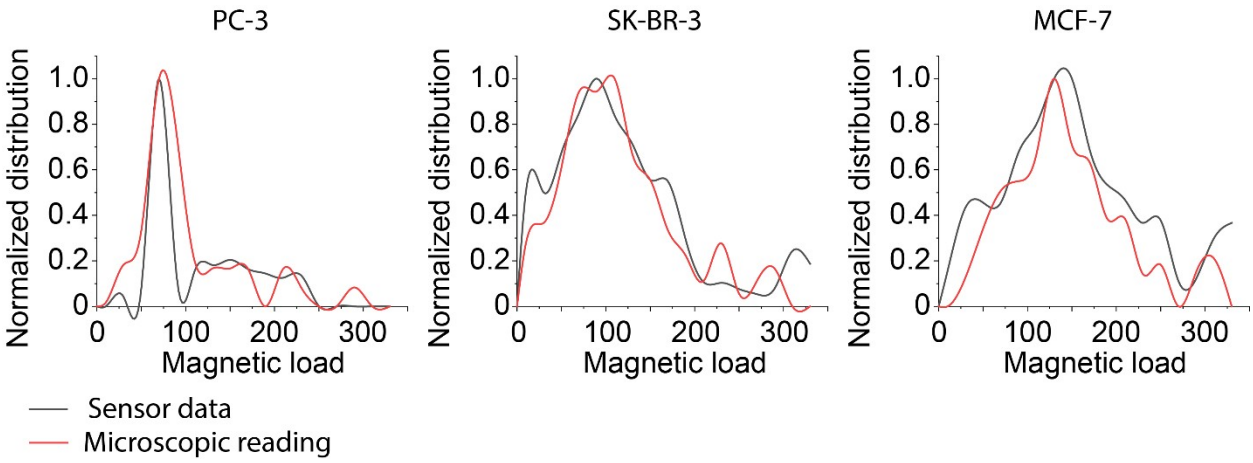

Supplementary Figure 3 | Validation of computational modeling and experimental measurements using the microscopic counting of magnetic load. The populations had correlation coefficients of 0.79, 0.90 and 0.91 for PC-3, SK-BR-3 and MCF-7 populations, respectively.

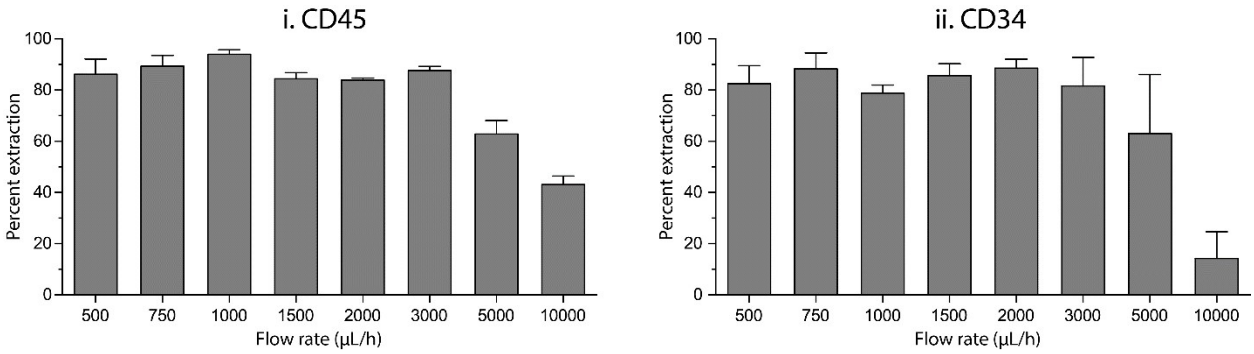

Supplementary Figure 4 | Validation of the optimal flow rate ranges with hematological cells. Magnetically labeled CD45+ and CD34+ samples were analyzed under various flow rates to identify the optimal flow conditions for experiments.

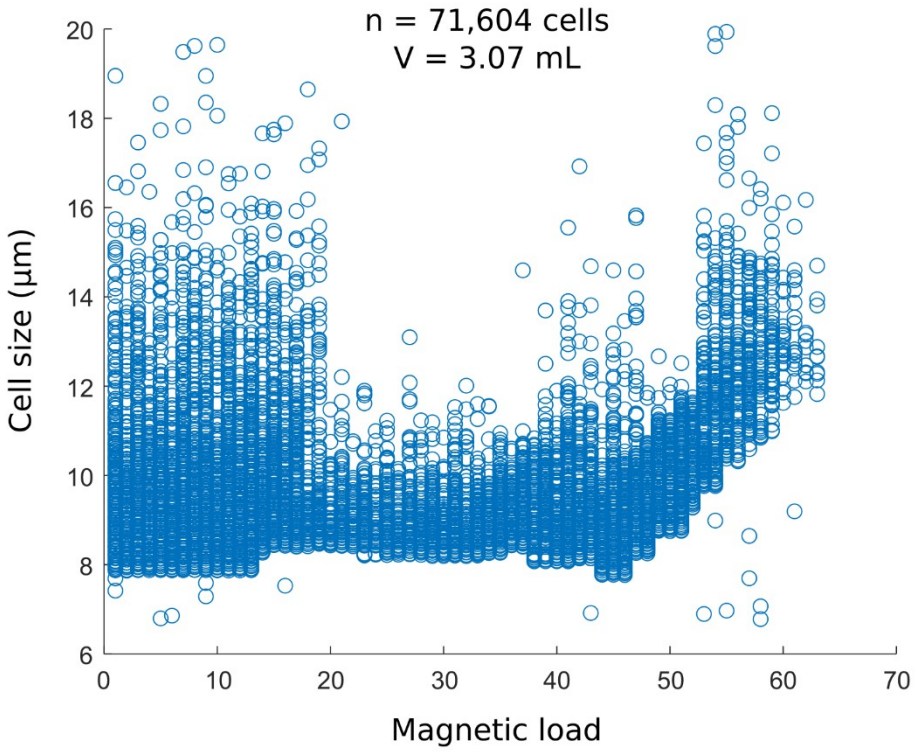

Supplementary Figure 5 | Results from the high-volume sample testing. 3mL of peripheral blood sample obtained from a healthy donor was labeled for CD34 and processed through the device in a single run at 1,500 µL/h flow rate. At the end of the analysis, a total of 71,604 CD34+ cells were recorded, yielding a density of 23.32 cells per µL. The cells also presented an average size of 8.82 µm, and a mean magnetic load of 39.41 beads.

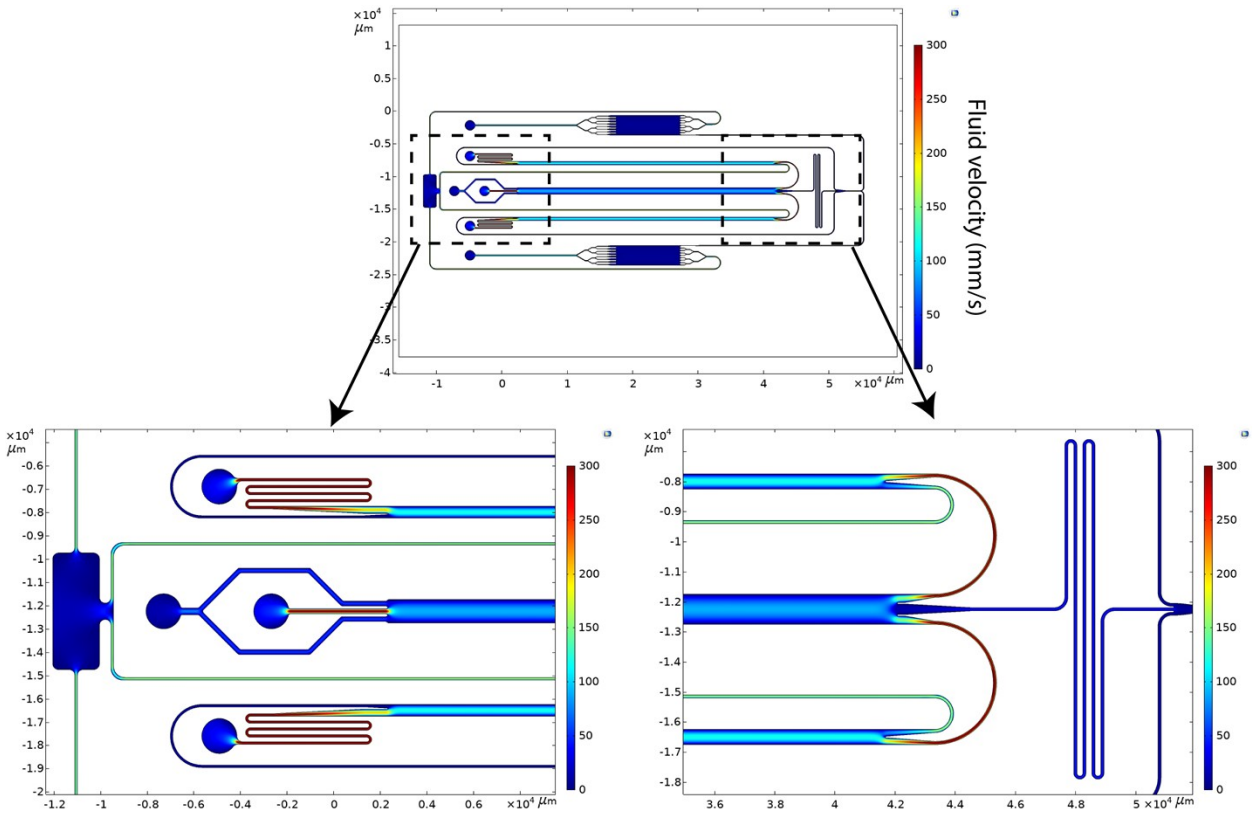

Supplementary Figure 6 | The velocity profile of the fluid flow in the device at 1000 µl/h. Insets show the zoomed in versions at the beginning and at the end of the central channel and the redundancy channels. The color bars have the unit of mm/s.

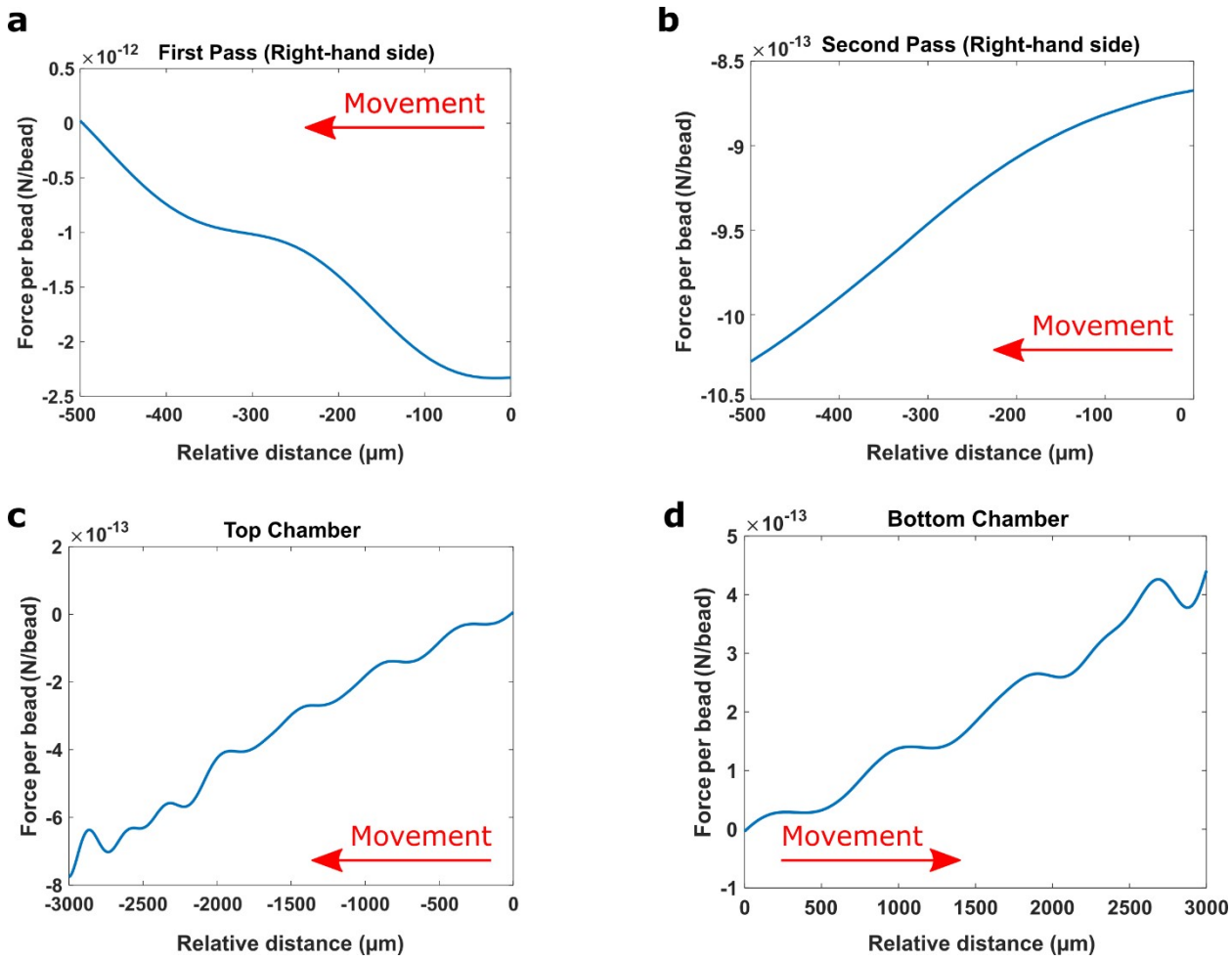

Supplementary Figure 7 | Magnetic forces in the transverse direction with respect to fluid flow for each region of the device. (**a**) Force profile of the first pass of the binary separation stage. Only the right-hand side is shown as both sides are symmetrical for the force profile with a sign difference. The magnetic force in the transverse direction becomes zero when the cell reaches the central streamline. (**b**) Force profile in the second (i.e. redundancy) pass. Both right and left redundancy channels have the same force profile, but in opposite directions. (**c**) Magnetic force vector acting on a cell based on the position of the cell in the top chamber. As the cell deflects more, the force acting on the cell increases. (**d**) Magnetic force vector for the bottom chamber for a given relative position of a cell in the chamber. Like the top chamber, there is a trend of an increasing magnetic force as the cell deviates further from original trajectory.

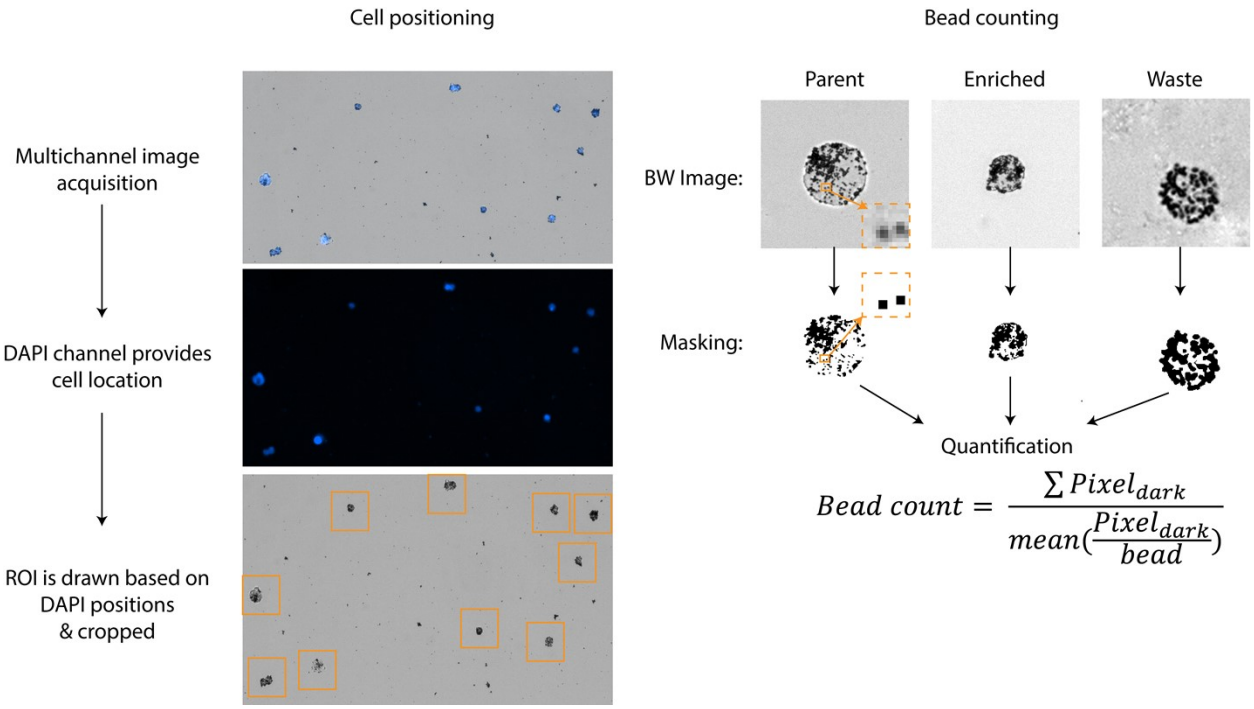

Supplementary Figure 8 | Image analysis of magnetic load. Cell populations were imaged under both DAPI and BF channels. DAPI channels identifies the location of target cells, and a corresponding region of interest was cropped from the BF channel. Then the images were binarized to quantify the number of beads.

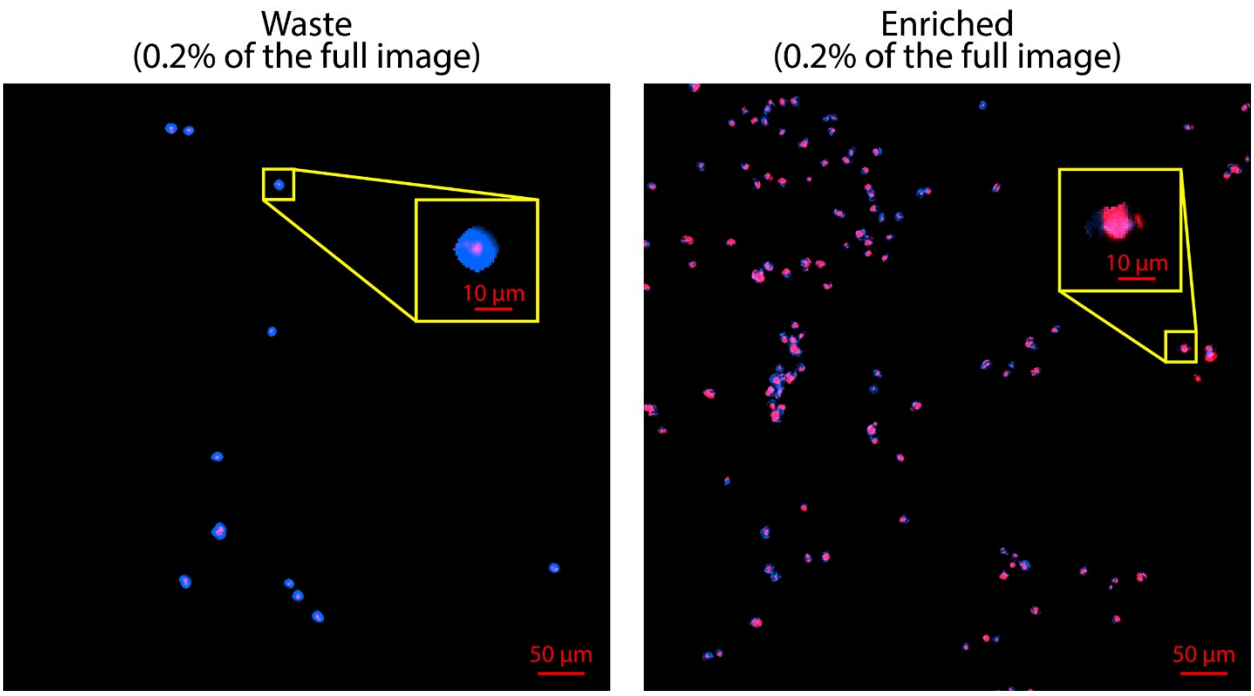

Supplementary Figure 9 | Outputs of the image processing program for a sample from the waste and from the enriched outlets. Waste outlet contained low expressors that were missed by magnetophoresis. The cells in the enriched sample displayed both wide ranges of surface expression. Only 0.2% of a whole processed image is shown here for a clearer visualization.

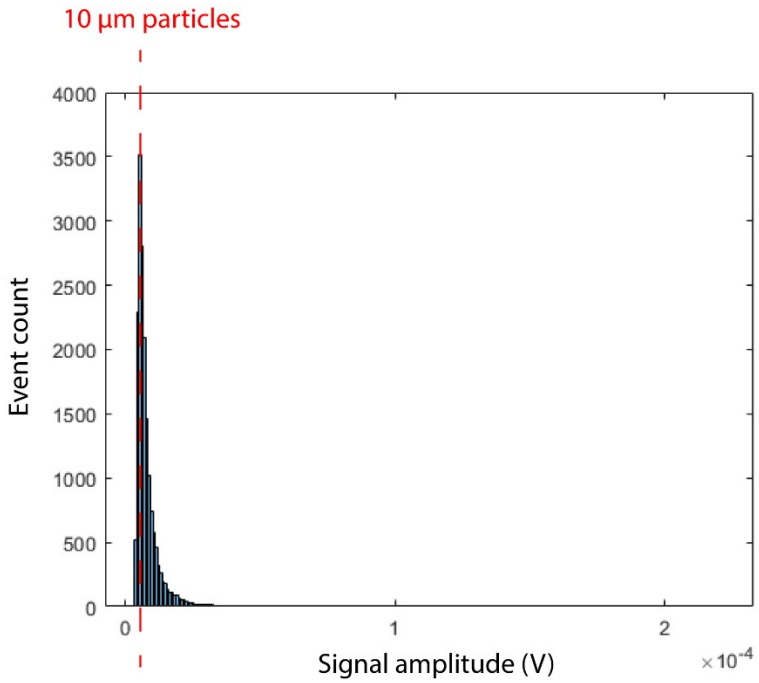

Supplementary Figure 10 | Size calibration of the electrical signals. 10 µm-sized polystyrene microspheres were used as the calibration agent. The mode of the amplitudes of the recorded signals was matched to the corresponding volume of the particles.

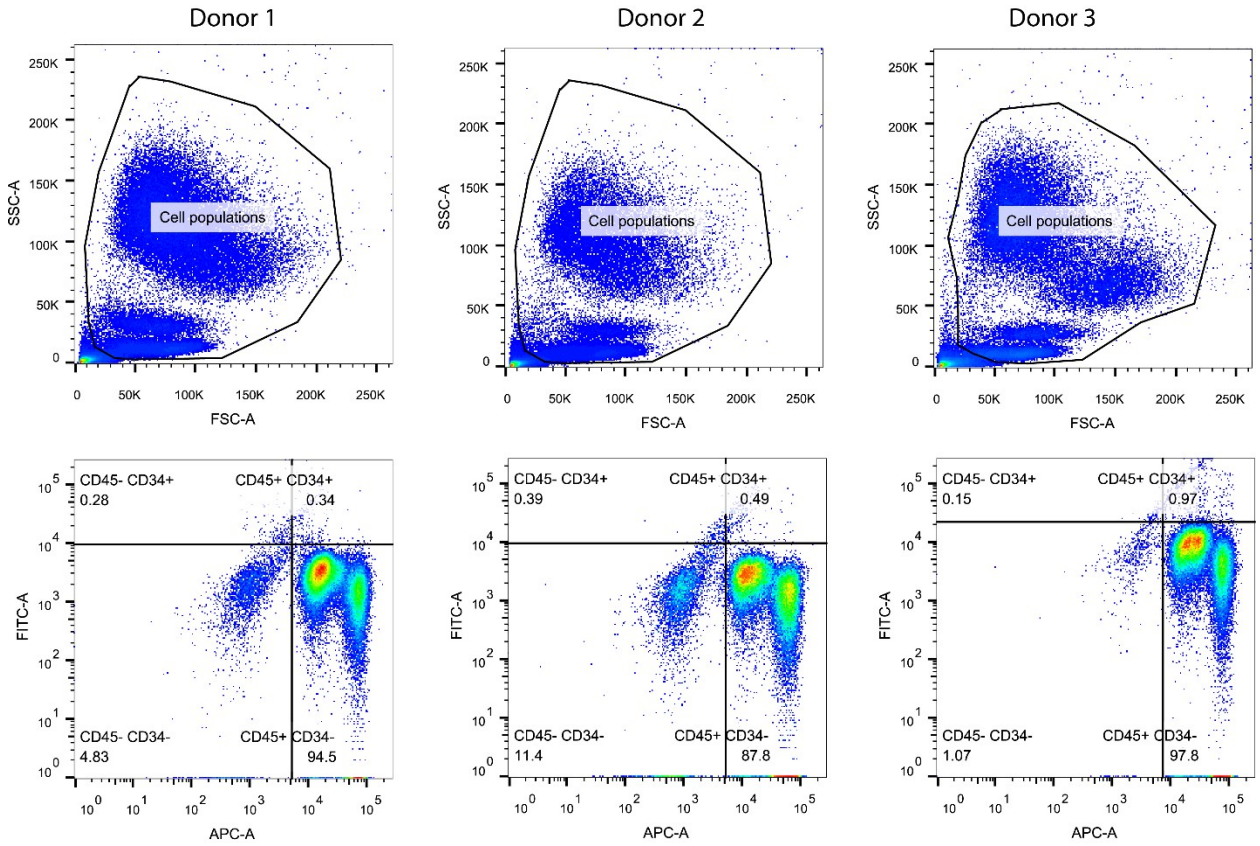

Supplementary Figure 11 | Gates used in the flow cytometry analysis of blood samples from donors. The analysis was done using a stain-lyse-no wash method, so the residue and debris were gated out first. Then, the target populations were identified using the APC-A (CD45) vs. FITC-A (CD34) graph.

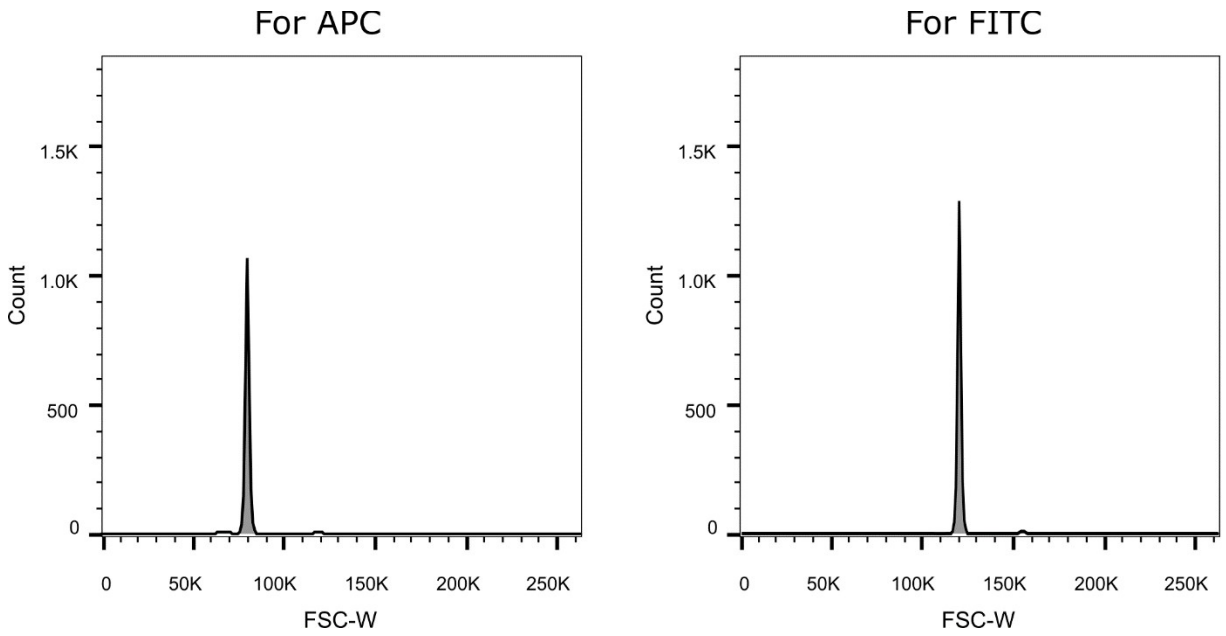

Supplementary Figure 12 | Calibration of the forward scatter width for cell size for APC and FITC-based analyses, separately. 10 μm polystyrene microspheres were analyzed under the same laser configurations as the experiment. The FSC-W value of the resulting peaks was set to represent the size of 10 μm.